RSC Advances

PAPER

View Article Online
View Journal | View Issue

Cite this: *RSC Adv.*, 2025, **15**, 34902

Synthesis of biogenic silver nanoparticles using *Piper chaba* leaf extract for dual-functional applications: Hg(II) sensing and catalysis

Aysha Siddika Akhe, Prianka Saha, Md. Rakibul Hasan Rakib, Nusrat Tazeen Tonu, Md. Ahsan Habib, Kaykobad Md. Rezaul Karim and Md. Mahiuddin *

This study reports the green synthesis of biogenic silver nanoparticles (AgNPs) for dual applications in mercury (Hg^{2+}) sensing and catalysis. AgNP formation was visually confirmed by a color change and corroborated by a surface plasmon resonance band at 441 nm in UV-vis spectra. FTIR spectroscopy, EDX, TGA, and DLS analyses confirmed phytochemical capping. XRD revealed a face-centered cubic structure with a crystallite size of 17 nm, while SEM and TEM showed monodispersed spherical AgNPs with an average size of 20 nm. The synthesized AgNPs exhibited high sensitivity for Hg^{2+} detection, with visual color changes and UV-vis shifts yielding low detection (14 ppm) and quantification (41 ppm) limits. Furthermore, the AgNPs demonstrated significant catalytic activity in reducing 4-nitrophenol to 4-aminophenol and degrading methyl orange and methylene blue dyes. This green synthesis offers a sustainable alternative to conventional methods for large-scale AgNP production, enabling selective Hg^{2+} detection in wastewater and showcasing its potential for environmental remediation and industrial catalysis.

Received 29th July 2025
Accepted 10th September 2025

DOI: 10.1039/d5ra05480j

rsc.li/rsc-advances

Introduction

Interest in nanotechnology is growing because of its numerous potential uses in a wide range of scientific fields.[1–3] Because of the recent rapid growth and expansion of technology, humans have placed their confidence in nanotechnology and believe it can increase their current lifestyle.[4–6] Metal nanoparticles (MNPs) are amazing components of nanotechnology with distinctive physicochemical features.[7–9] Scientists have thus focused their attention and study on ensuring that MNPs are used in a more acceptable and profitable manner in a variety of disciplines, including electronics, medicine, agriculture, and water purification. With their low toxicity, ease of synthesis, controlled products, and versatile uses, silver nanoparticles (AgNPs) are one of the most remarkable metal nanoparticles (MNPs) and are the subject of this study.[10–12]

Mercury (Hg) is a widely recognized acute element that poses a significant risk to human health and the environment.[13,14] As a result, identifying Hg^{2+} ions is crucial in order to remove them from food and water. Many sensing methods, including atomic absorption spectrometry (AAS), atomic emission spectrometry (AES), and inductively coupled plasma mass spectrometry (ICP-MS), have been used to detect high concentrations of Hg^{2+} ions.[15–18] However, because these technologies require costly equipment and intricate methods, they are not very useful for rapid on-site investigations. To address these drawbacks, biomaterial-based colorimetric sensors for Hg^{2+} detection have been developed. Among various materials, nanoparticles have shown considerable promise as a sensing probe.[19–23]

Additionally, organic pollutants have a detrimental effect on the environment, particularly on water, and are still discharged from many factories as discharge effluents. These pollutants are harmful to human and animal health since they may lead to a variety of illnesses, such as blood problems, skin irritation, liver and kidney damage, and poisoning of the central nervous system.[24–26] Organic dyes are a significant and representative subset of organic pollutants that also poses a considerable threat to aquatic ecosystems and human health.[26–29] Their widespread use in industries such as textiles and paper makes them a major source of persistent, highly visible, and often toxic water pollution. Thus, it has become essential to remove organic dyes from water. Adsorption and degradation are two important techniques to remove such organic dyes.[30,31] The degradation of organic dyes is much simpler, faster, and more consistent than their adsorption-based removal. Organic dyes undergo degradation to become less harmful components.[32] However, the main obstacle in turning these chemicals into harmless products is their great stability. Certain nanocatalysts have demonstrated their capacity to accelerate the breakdown of these organic dyes into colorless, harmless byproducts *via* a sustainable procedure.[33–35]

Chemistry Discipline, Khulna University, Khulna 9208, Bangladesh. E-mail: mahiuddin@chem.ku.ac.bd

Among the noble metal nanoparticles, AgNPs are considered remarkable and one of the most frequently used nanocatalysts to degrade organic dyes.[36,37] Thus, a prime focus of this study is to utilize AgNPs to serve a dual purpose: first, as an efficient catalyst for the degradation of organic dye molecules, and second, as a highly sensitive sensing nanoprobe for detecting toxic heavy metals like mercury in the same wastewater. This dual-functionality highlights the innovation of our approach, showcasing a single material that can address multiple types of water contaminants simultaneously, thereby providing a more comprehensive and synergistic solution for water treatment.

The literature indicates that green approaches are thought to be good alternatives for traditional chemical methods in the synthesis of AgNPs because they do not use any hazardous chemicals, making them environmentally friendly, and in line with the UN's sustainable development goals (SDGs).[38–40] Moreover, green-synthesized AgNPs have demonstrated their value as nanocatalysts for the degradation of organic dyes[30,33,37,41,42] and as nanoprobes for the detection of Hg^{2+} ions.[19,20,43,44] AgNPs are synthesized using the aqueous extract of various plant sources, including *Sargassum serratifolium*,[42] *Cucumis sativus* and *Aloe vera* leaf,[37] green coffee bean,[45] *Biophytum sensitivum* leaf,[46] *Gmelina arborea* fruit,[47] and *Thymbra spicata* leaf,[48] and used as a nanocatalyst for the reduction of organic dyes. Moreover, AgNPs are synthesized using the aqueous extract of various plant sources, including citrus fruit,[44] *Viburnum opulus* fruit,[30] *Securidaca inappendiculata* Hassk stem,[21] and *Piper chaudocanum* stem,[20] and used as a nanoprobe for the colorimetric detection of Hg^{2+}. *Trigonella foenum-graecum* leaf,[49] *Artemisia vulgaris*,[50] and *Bistorta amplexicaulis* root[43] are also used to synthesize AgNPs as a nanocatalyst for the degradation of organic dyes and as a nanoprobe for the detection of Hg^{2+}. Meanwhile, our research group has also employed *Citrus macroptera* fruit peel[51] and *Piper chaba* stem[33] to synthesize AgNPs, and used them as a nanoprobe for the detection of Hg^{2+} ions and as a nanocatalyst for the degradation of organic dyes. The utilization of redundant plant sources for the production of AgNPs as both a nanoprobe and a nanocatalyst is one of the main interests of this study.

According to the literature, *Piper chaba* includes a variety of chemicals, the most common of which are alkaloids and lignan,[52–54] which may be able to convert Ag^{+} into Ag^{0}. From the existing literature, no AgNPs have been synthesized using *Piper chaba* leaves. Thus, the primary objectives of this work are to establish the ideal synthetic conditions for the synthesis of AgNPs using the leaf extract of *Piper chaba*, and then use the resultant AgNPs as a powerful and efficient nanoprobe for the colorimetric detection of Hg^{2+} ions and as a promising nanocatalyst for the degradation of organic dyes.

Experimental

Collection of plant materials

Piper chaba leaves were collected from the Khulna District of Bangladesh. To remove impurities, the leaves were first washed with normal tap water and then deionized distilled water (DDW). Then, the leaves were dried at room temperature for 3–4 days and crushed into a powder.

Preparation of plant extract

Crushed leaves (20 g) were placed in a round-bottom flask containing 200 mL of DDW and boiled for 40 min. After cooling to room temperature, the mixture was first filtered through muslin cloth, followed by filtration using Whatman No. 1 filter paper. The resulting solution was then centrifuged at 11 000 rpm for 10 min to obtain the final extract, which was stored at 4 °C for subsequent use.

Materials

$AgNO_3$ was purchased from Merck Chemicals (Merck KGaA, Darmstadt, Germany). $BaCl_2 \cdot 2H_2O$ was purchased from BDH, UK, while $NiCl_2 \cdot 6H_2O$, $CoCl_2 \cdot 6H_2O$, and $CdSO_4 \cdot 8H_2O$ were procured from Loba Chemie, India. $Mg(NO_3)_2 \cdot 6H_2O$, $Pb(NO_3)_2$, and $FeSO_4 \cdot 7H_2O$ were obtained from Merck, India, and $HgCl_2$ was procured from Molychem, India. 4-Nitrophenol (4-NP) was purchased from Tokyo Chemical Industry Co., Ltd. (Tokyo, Japan), while methylene blue (MB), methyl orange (MO), and sodium borohydride ($NaBH_4$) were procured from Kanto Chemical Co., Inc. (Tokyo, Japan).

Green synthesis of silver nanoparticles (AgNPs)

The synthesis conditions were optimized by adjusting certain parameters such as the temperature, pH, reaction time, amount of plant extract, and $AgNO_3$ concentration, while keeping the other variables constant. AgNPs were then synthesized under the prescribed conditions. A 2 mM aqueous solution of $AgNO_3$ (100 mL) was placed in a volumetric flask. To prevent the silver from oxidizing, the flask was wrapped with carbon paper. 2 mL of *Piper chaba*'s aqueous leaf extract was placed in a conical flask. A 2 mM (40 mL) $AgNO_3$ solution was added to the flask containing the *Piper chaba* leaf extract. With continuous stirring, the mixture was heated for 60 min at 80 °C in an oil bath. The solution changed from colorless to reddish-brown when the *Piper chaba* leaf extract was added throughout this procedure, indicating the formation of AgNPs. The resulting dispersion was allowed to settle at room temperature for 12 h. The AgNPs reaction mixture was then centrifuged for 30 min at 11 000 rpm in the centrifuge machine. To get rid of contaminants, the precipitate was washed three times with DDW.

Measurements

UV-vis spectroscopic analyses were conducted using a SHIMADZU UV-1900i UV-vis spectrophotometer, with the absorption spectra recorded at a resolution of 1 nm over a wavelength range of 200–800 nm. X-ray diffraction (XRD) analysis was conducted on a Rigaku Ultima IV RINT D/max-kA spectrometer (Tokyo, Japan) using Cu-Kα radiation. FTIR spectra were obtained at 25 °C using a KBr pellet on a JASCO FT/IR-460 Plus spectrometer (Tokyo, Japan), with a scanning rate of approximately 4 cm^{-1} s^{-1}. Thermogravimetric analysis (TGA) was performed using a SHIMADZU TGA-50 instrument (Tokyo, Japan)

at a heating rate of 10 °C min^{-1} under a nitrogen atmosphere. The average hydrodynamic diameters were measured using a NICOMP particle sizer (Entegris, CA, USA) *via* dynamic light scattering. Field emission scanning electron microscopy (FE-SEM) and energy-dispersive X-ray (EDX) analysis were carried out on a Hitachi SU-8000 microscope (Tokyo, Japan) at accelerating voltages of 5 and 10 kV. Transmission electron microscopy (TEM) measurements were performed using a JEOL TEM-2100F field emission electron microscope (Tokyo, Japan).

Colorimetric detection of mercury (Hg^{2+})

The colorimetric detection of Hg^{2+} was carried out using the identical procedure described in our previous report.[19] Several metal ion stock solutions having different concentrations were prepared, and AgNPs were added to them in an equal amount to serve as a colorimetric probe. The absorbance was then recorded using a UV-vis spectrophotometer, and the outcome was assessed using ultrapure water as a control sample. Metal ions solutions, including Ba^{2+}, Co^{2+}, Cd^{2+}, Fe^{2+}, Hg^{2+}, Mg^{2+}, Ni^{2+}, and Pb^{2+} (1.5 mL, 90 μM), were added to the detection system (1.5 mL of AgNPs) to evaluate the selectivity. AgNPs, Hg^{2+} (90 μM), and interfering metal solutions (Ba^{2+}, Co^{2+}, Ni^{2+}, Cd^{2+}, Mg^{2+}, Pb^{2+}, and Fe^{2+}) (90 μM) were mixed in an equal proportion to simulate the effects of additional interfering metal ions. The total volume of the mixture's was kept constant (10 mL). Also, under the same circumstances, the AgNPs probe evaluated various quantities of Hg^{2+} samples (10 to 90 μM) to assess the probe's accuracy. After mixing all of the test samples, they were to be held for 10 min before the absorption was measured. To determine the concentration of Hg^{2+}, the measured absorption was transformed into a linear equation. Based on the following equation, the limit of detection (LOD) and limit of quantification (LOQ) of the Hg^{2+} colorimetric detection by the synthesized AgNPs were determined:[20]

$$\mathrm{LOD} = (3 \times S_i)/b \quad (1)$$

$$\mathrm{LOQ} = (10 \times S_i)/b \quad (2)$$

where, S_i = standard deviation of the intercept and b = slope of the linear fitting.

Catalysis

The catalytic reduction of 4-NP was carried out by adding 1.5 mL of a freshly prepared aqueous $NaBH_4$ solution (20 mM) to 2 mL of an aqueous 4-NP solution (22 ppm), followed by the addition of 10 μL of colloidal AgNPs dispersion (0.5 mg mL^{-1}). The reaction progress was monitored at 25 °C by recording the UV-vis absorption spectra over time. Control experiments were conducted under identical conditions, but without the addition of AgNPs. Similarly, the catalytic reduction of MO and MB was performed by mixing 2 mL of aqueous MO (15 ppm) or MB (10 ppm) with 1.5 mL of freshly prepared aqueous $NaBH_4$ solution (20 mM) and 10 μL of colloidal AgNPs dispersion (0.5 mg mL^{-1}).

Results and discussion

One special and fascinating technique for assessing the formation of silver and gold nanoparticles as a preliminary indication is visual inspection, which is also completely free of cost. Here, the development of AgNPs *via in situ* reduction and coating with the likely phytochemicals of *Piper chaba* leaf is demonstrated by the observation of the color shift of the reaction mixture including $AgNO_3$ and *Piper chaba* leaf extract from almost colorless to reddish-brown (Fig. 1). UV-vis spectroscopy is a useful technique to verify AgNPs production and estimate particle size after visual investigation. AgNPs production is indicated by the emergence of the surface plasmon resonance (SPR) band, and the particle size is predicted by the location of the SPR band. The synthesized product's UV-vis spectrum (Fig. 1) revealed an SPR band at 441 nm, which is located in a region that is characteristic of AgNPs.[33] This observation confirms that AgNPs were formed in the reaction mixture as a result of Ag^+ ions being reduced by the likely phytochemicals found in the *Piper chaba* leaf extract.

Many variables, including the temperature, pH, reaction duration, silver salt concentration, and the presence of reducing and stabilizing chemicals, are important in the synthesis of stable AgNPs. As a result, factors including the temperature, pH, reaction duration, plant extract concentration, and silver ion concentration would all have an impact on the synthesis utilizing plant sources. By keeping the reaction volume constant, the aforementioned factors were examined to optimize the synthetic condition and progress was monitored by UV-vis spectroscopy.

The mixture of 40 mL of 2 mM $AgNO_3$ and 2 mL of leaf extract was used in the reactions, which were run for a duration of 10 to 180 min at 80 °C while maintaining a pH of 6.1 (without further adjusting). This allowed for the evaluation of the impact of the reaction time. The UV-vis spectra of the AgNPs produced over

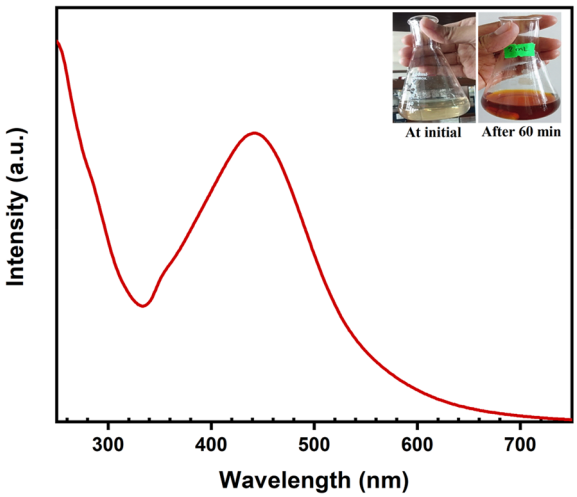

Fig. 1 UV-vis spectrum of a reaction mixture of $AgNO_3$ (40 mL of 2 mM) and *Piper chaba* leaf extract (2 mL of 1 g/10 mL) after 60 min of reaction time at 80 °C with (inset) the visual appearance of the reaction mixture at the initial state and after 60 min.

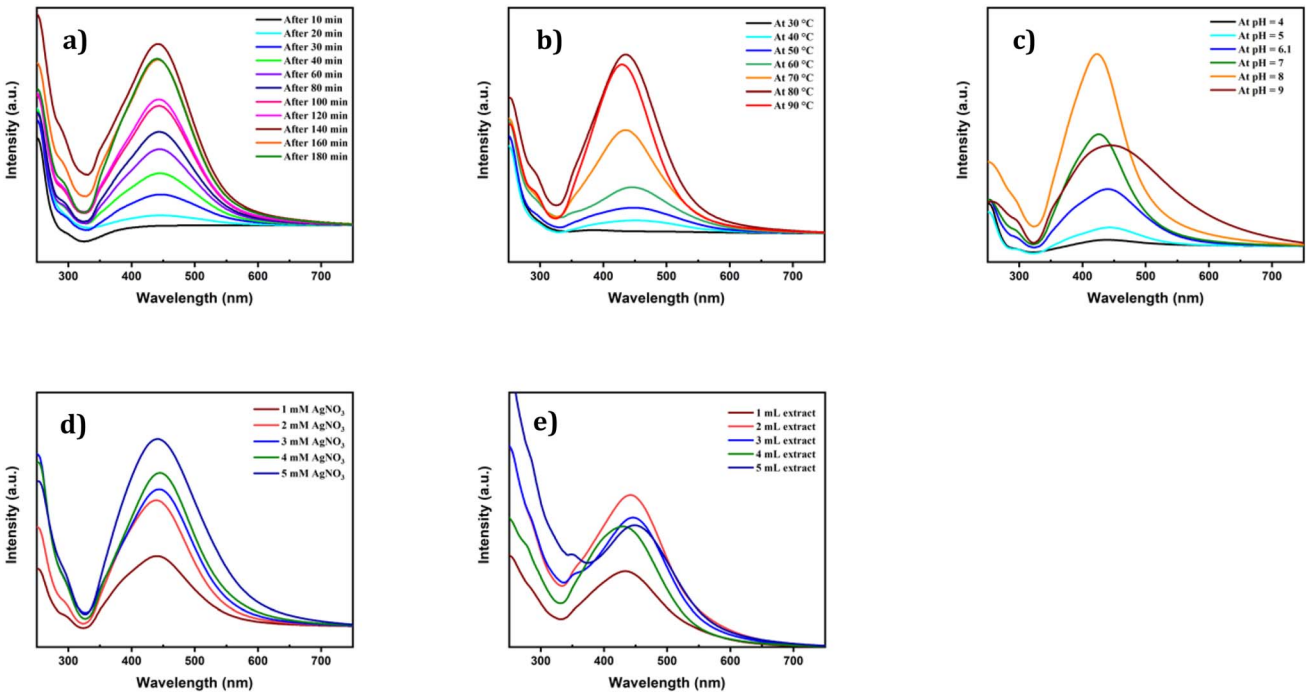

Fig. 2 UV-vis spectra of AgNPs synthesized using *Piper chaba* leaf extract under various conditions: (a) time; (b) temperature; (c) pH; (d) concentration of $AgNO_3$; and (e) concentration of leaf extract to optimize the synthetic conditions.

a period of 10 to 180 min are shown in Fig. 2a. It demonstrates that the SPR band of AgNPs was first observed as a broad peak after 20 min. As time passed, the peak sharpened and intensified, indicating the gradual formation of AgNPs.[55–58] However, after 140 min, the peak's intensity decreased, most likely as a result of AgNPs aggregation. While a maximum intense peak was seen at 140 min of reaction time, good intense peaks were also observed at lower reaction times. Thus, 60 min was set as the optimal reaction time when considering time management.

The mixture of 40 mL of 2 mM $AgNO_3$ and 2 mL of leaf extract was used in the reactions, and the pH was kept at 6.1 (without any additional adjustments) for 1 h at a temperature range of 30 to 90 °C in order to assess the impact of temperature. The UV-vis spectra of the AgNPs synthesized between 30 and 90 °C are shown in Fig. 2b. It can be seen that the sharpness and intensity of the SPR band increased with temperature, suggesting an acceleration of the reduction.[41,59] The SPR band's intensity decreased beyond 80 °C. The possible cause of this decline in peak intensity might be the AgNPs' aggregation.[41,55] Nevertheless, the SPR band showed a blue shift over 60 °C. Such a change might be the result of faster reduction, leading to the production of smaller particles.[56]

A mixture of 40 mL of 2 mM $AgNO_3$ and 2 mL of leaf extract was used in the reactions for 1 h at 80 °C at a pH range of 4 to 9, using HCl and/or NaOH to adjust the desired pH. This made it possible to assess how pH affected the formation of AgNPs. Fig. 2c displays the UV-vis spectra of the AgNPs generated across a pH range of 4 to 9. It shows that AgNPs' SPR band was only marginally visible at pH 4, which suggests that AgNPs were not significantly formed. It is possible that the increased acidity is inappropriate for phytochemicals to execute their reducing capacity.[55,60] The sharpness and intensity of the SPR band increased with increasing pH, suggesting rapid reduction of Ag^+ ions and formation of AgNPs. Such fast reduction may result from the phytochemicals' enhanced reducing ability.[61] Furthermore, the change in intensity and sharpness of the SPR band at pH 6.1 and 7 was drastic, and the maximum intensity was observed at pH 8. Beyond pH 8, the SPR band's intensity dropped. The aggregation of AgNPs may be the reason for this drop in peak intensity. However, to avoid the use of additional chemicals to adjust the pH of the reaction mixture and to take environmental concerns into account, the pH obtained in the reaction mixture after the addition of $AgNO_3$ and leaf extract, which is ~6.1, was selected as the optimal pH.

A mixture of 40 mL of 1 to 5 mM $AgNO_3$ and 2 mL of leaf extract was used in the reactions, and the pH was kept at 6.1 (without any additional adjustments) for 1 h at 80 °C in order to assess the impact of the $AgNO_3$ concentration. The UV-vis spectra of the AgNPs synthesized using different concentrations of $AgNO_3$ are shown in Fig. 2d. The UV spectra showed that when the concentration of $AgNO_3$ grew, the SPR band's intensity increased as well, suggesting that many AgNPs were being formed.[41,55,60] The SPR band somewhat redshifted beyond 2 mM. Such a red-shift might be caused by aggregation. However, the SPR band's intensity does not grow in the same proportion from 1 mM to 2 mM. The phytochemicals found in 2 mL of extract may be in excellent proportion to the Ag^+ ions in 2 mM 40 mL $AgNO_3$. Therefore, the optimum concentration of $AgNO_3$ should be considered as 2 mM.

The mixture of 40 mL of 2 mM $AgNO_3$ and 1 to 5 mL of leaf extract was used in the reactions, and the pH was kept at 6.1 (without any additional adjustments) for 1 h at 80 °C in order to

assess the impact of the leaf extract concentration. Fig. 2e displays the UV-vis spectra of the AgNPs that were created with varying extract concentrations. The UV spectra revealed that the SPR band's maximum intensity was attained at 2 mL, suggesting that utilizing 2 mL of extract resulted in the right ratio of Ag^+ ions and reducing phytochemicals. However, the SPR band's intensity dropped and slightly redshifted beyond this volume. The aggregate might be the reason for such a red shift. Therefore, it was thought that using 2 mL of leaf extract was ideal.

The total optimization findings make it clear that the reaction should be carried out by combining 40 mL of 2 mM $AgNO_3$ and 2 mL of extract (1 g/10 mL), while keeping pH 7 at 80 °C for 1 h. This would yield high-quality AgNPs.

XRD examination proved the resulting product's crystalline nature and phase purity. The dried AgNPs' XRD pattern, which was synthesized using *Piper chaba* leaf extract, is displayed in Fig. 3. Based on the XRD pattern, four distinct diffraction peaks with 2θ values of 38.12°, 44.26°, 64.24°, and 77.56° were identified. These peaks correspond to the lattice planes of (111), (200), (220), and (311), respectively, and are well indexed with the elemental Ag face-centered cubic phase (JCPDS file no. 04-0783). Moreover, diffraction peaks at 27.87°, 32.25°, 38.12°, 46.24°, and 57.54° correspond to the lattice plane of (110), (111), (121), (200), and (311), respectively, and are also well indexed with the elemental Ag face-centered cubic phase (JCPDS file no. 84-0713). These findings suggest that the final product is AgNPs lacking noticeable oxide phases. However, a few unidentified peaks (55.48°, 67.85°, and 74.76°) can be found in the XRD pattern; these are most likely impurities of the AgCl phase and the organic coating with crystalline phases.[33,41,62,63] Applying Scherrer's equation to the diffraction peaks of the (110), (111), and (200) planes yielded the average crystallite size of 17 nm. The crystallinity and micro-strain were found to be 90.75% and 1.34×10^{-3}, respectively, indicating the high crystallinity of the prepared AgNPs. Bragg's law was used to calculate the *d*-spacing, listed in Table 1. This finding suggests that the *Piper chaba* leaf phytochemicals can reduce silver salts and create AgNPs.

Table 1 Calculated *d*-spacing of the prepared AgNPs

		(*h k l*)	
2 theta	*d*-Spacing (Å)	JCPDS: 04-0783	JCPDS: 84-0713
27.87	3.190786717		(1 1 0)
32.12	2.766005296		(1 1 1)
38.12	2.352902950	(1 1 1)	(1 2 1)
44.26	2.039561692	(2 0 0)	
46.24	1.957756393		(2 0 0)
55.48	1.669903601		
57.54	1.598949923		(3 1 1)
64.24	1.440762725	(2 2 0)	
67.85	1.385056561		
74.76	1.271146444		
77.56	1.233614829	(3 1 1)	

FTIR spectroscopy analysis was carried out to investigate the structure of the organic moieties covering the surface of AgNPs. The FTIR spectra of the AgNPs produced using *Piper chaba* leaf extract and the solid content of leaf extract are shown in Fig. 4. Both spectra had a wide peak at 3393 cm^{-1}, attributed to the stretching vibrations of the O–H and N–H bonds. The lower wavenumber region of the AgNPs spectrum had a broad shoulder, suggesting that hydrogen bonds have formed between the AgNPs surface and the O–H and N–H bonds in the organic molecules that capped them. There were no observable signals at 3000 cm^{-1}, indicating that the number of aromatic and alkenyl protons may be quite small. The stretching vibration of C=O as a small signal at 1715 cm^{-1} and C=O as a strong band at 1605 cm^{-1} are assignable to ester and/or carboxy groups and amides, respectively, which exist in *Piper chaba*.[64–66] The methyl group C–H stretching, C–O–H bending, and C–O stretching are represented by the bands found at 1455, 1373, and 1046 cm^{-1}, respectively. These characteristics are

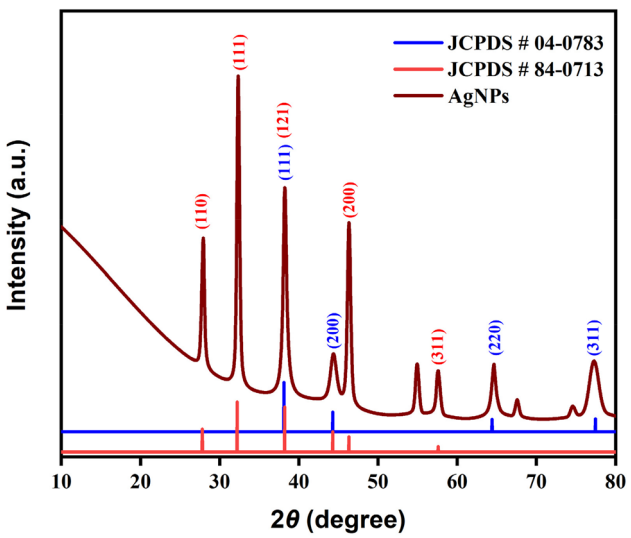

Fig. 3 XRD pattern of AgNPs synthesized using 40 mL of 2 mM $AgNO_3$ and 2 mL of *Piper chaba* leaf extract (1 g/10 mL) at pH 7 and 80 °C for a reaction time of 1 h.

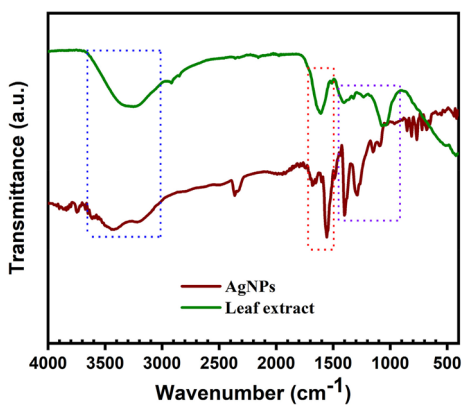

Fig. 4 FTIR spectra of the solid content of *Piper chaba* leaf extract and AgNPs synthesized using 40 mL of 2 mM $AgNO_3$ and 2 mL of *Piper chaba* leaf extract (1 g/10 mL) at pH 7 and 80 °C for a reaction time of 1 h.

consistent with plant-derived polysaccharides. The capping chemicals are most likely polysaccharides, amide and hydroxy groups, carboxy, carboxylate, and/or ester moieties, according to the FTIR spectroscopy data. The potential structures for capping compounds are validated by this FTIR spectroscopic data. As we previously reported,[33] the absence of such distinctive FTIR peaks in the spectrum of AgNPs prepared in the absence of a stabilizing agent suggests that the capping compounds are derived from *Piper chaba* leaf extract.

The surface of AgNPs had some organic moieties acting as capping agents, as shown by the FTIR analysis. Nevertheless, thermogravimetric analysis (TGA) was used to determine the relative quantity of these organic moieties. Fig. 5 shows the TGA curve of AgNPs produced with *Piper chaba* leaf extract. It shows that 8% of the weight loss took place at a temperature range of 190–440 °C, which was mostly connected with the AgNPs surface's organic moieties degrading. The AgNPs are well-stabilized due to the presence of such organic moieties on the surface of AgNPs.

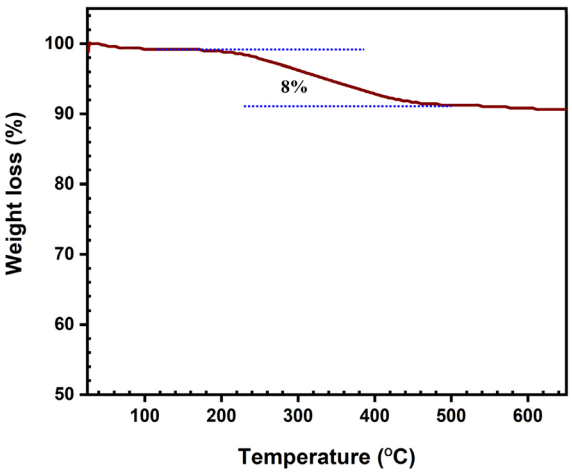

Fig. 5 TGA curve of AgNPs synthesized from 40 mL of 2 mM $AgNO_3$ and 2 mL of *Piper chaba* leaf extract (1 g/10 mL) at pH 7 and 80 °C for a reaction time of 1 h.

The FE-SEM image (Fig. 6) at the high magnification range (100 nm) shows the dense, random, and compressed distribution of quasi-spherical nanoparticles with sizes between 15 and 20 nm. This growth of nanoparticles approximately aligned with the growth of AgNPs utilizing *Fusarium solani* extracted from infected tomato plants.[67]

The elemental composition of green synthesized AgNPs, particularly the capping of phytochemicals, may be better understood using EDX analysis. The EDX spectrum (Fig. 7) of the green synthesized AgNPs made using *Piper chaba* leaf extract confirms that silver (69%) and carbon (10%), as well as oxygen (8%), are present. As expected, the carbon and oxygen signals corroborated the findings of the FTIR and TGA data, and suggested the existence of phytochemicals along with Ag in the synthesized AgNPs. The carbon and oxygen peaks' notable intensities suggest that the AgNPs have a substantial coating layer.

The TEM image (Fig. 8a) shows the formation of AgNPs with a primarily spherical morphology. The particles have a size distribution between 10 nm and 50 nm, and most look evenly distributed and well-separated. The histogram (Fig. 8b) shows that the particles have an average size of 20.10 nm. The TEM image at high resolution (Fig. 8c) was taken and a small section was selected and analyzed. The corresponding FFT graph and its profile plot are shown in Fig. 8d and e, respectively. The *d*-

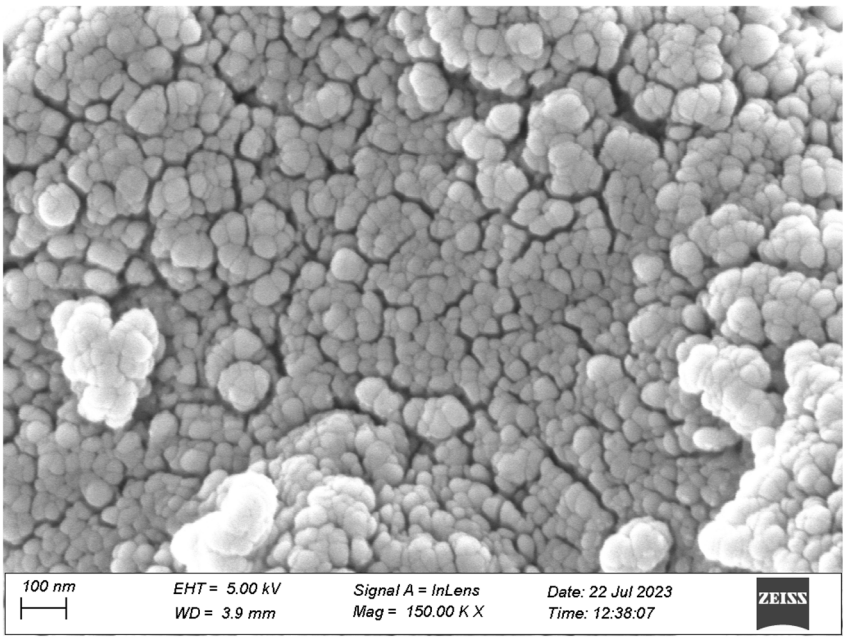

Fig. 6 FE-SEM image of AgNPs synthesized from 40 mL of 2 mM $AgNO_3$ and 2 mL of *Piper chaba* leaf extract (1 g/10 mL) at pH 7 and 80 °C for a reaction time of 1 h.

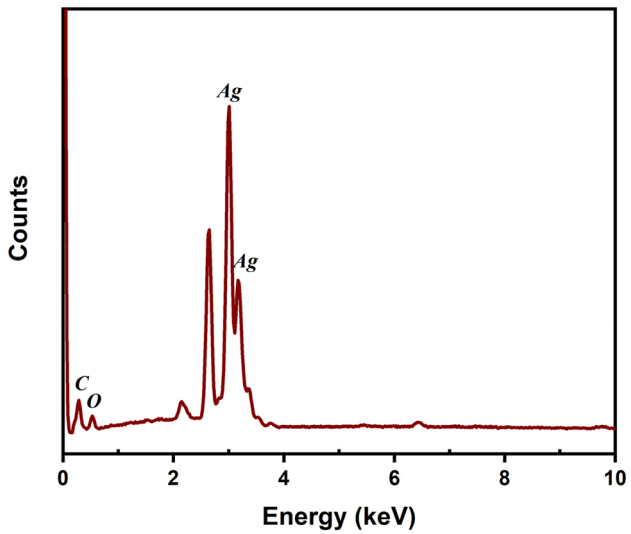

Fig. 7 EDX spectrum of AgNPs synthesized from 40 mL of 2 mM $AgNO_3$ and 2 mL of *Piper chaba* leaf extract (1 g/10 mL) at pH 7 and 80 °C for a reaction time of 1 h.

spacing was found to be 0.234 nm, which is very close to the calculated value for plane (111) of JCPDS: 04-0783, determined from XRD data. The non-aggregated spherical shapes reported in this paper probably result from the controlled synthesis technique using *Piper chaba* leaves extract green reducing agent. Negligible aggregation hints at the existence of effective capping agents, which serve to efficiently stabilize the nanoparticles maintaining their individual structure. The fact that the AgNPs have a relatively uniform size and morphology is important to a number of applications, for example, high surface area and nanoscale dimensions (critical for antimicrobial activity and catalytic activity). The lack of major morphological defects features supports the applicability of the product synthesis method. Moreover, the synthesis procedure is validated by the reproducible dispersion along with separate boundaries. This reflects the possibility of using environmental techniques to synthesize nanoparticles of high quality with application in industry and biomedicine.

AgNPs' hydrodynamic diameter was assessed using the DLS technique. AgNPs were found to have an average hydrodynamic diameter (D_h) of 110 nm, which is greater than the sizes determined by SEM and TEM studies. AgNPs made using *Citrus macroptera* peel extract[41] and *Piper chaba* stem extract[33] showed a comparable difference. As in the previously reported works, a hydrated layer made up of swelling organic moieties on the surface of AgNPs in Brownian motion may be the cause of the larger particle size.

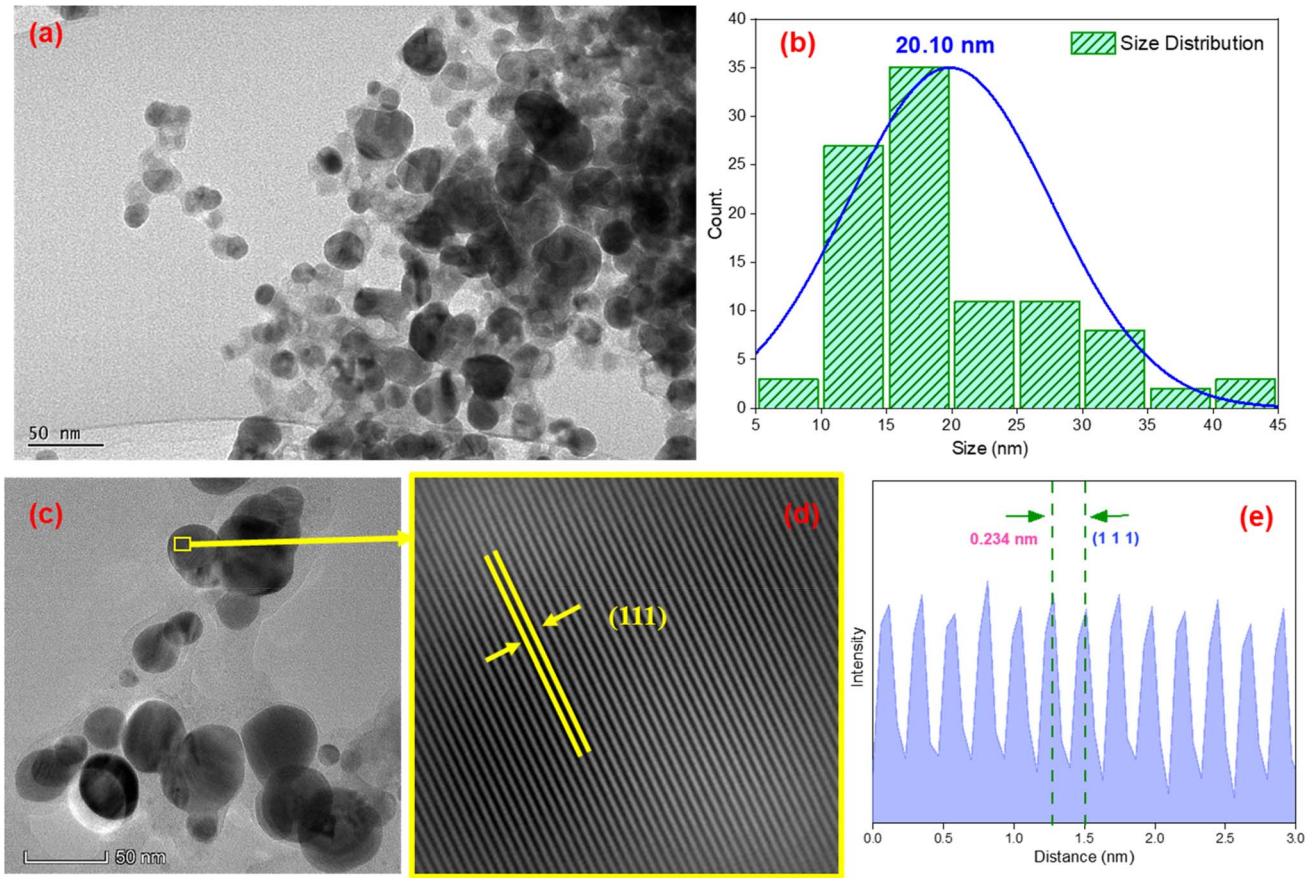

Fig. 8 (a) TEM image of AgNPs synthesized from 40 mL of 2 mM $AgNO_3$ and 2 mL of *Piper chaba* leaf extract (1 g/10 mL) at pH 7 and 80 °C for a reaction time of 1 h, the (b) corresponding histogram, (c) TEM at 50 nm scale, (d) FFT graph of the selected area of (c), and the (e) corresponding profile plot.

Hg^{2+} detection using synthesized AgNPs

The oxidation of elemental Ag or AgNPs aggregation caused by Hg^{2+} ions is the basis for the detection principle. When Hg^{2+} is not present, the AgNPs stay scattered and display distinctive optical or electrochemical characteristics.[21–23,47] Nevertheless, Hg^{2+} interacts with AgNPs' surface upon addition, causing oxidation or aggregation. The optical approach has been used in this investigation to assess such detection by comparing the color of the solution and the change in the UV-vis absorption spectrum before and after the addition of Hg^{2+}. AgNPs oxidation or aggregation usually causes a change in the absorption peak, which is observed by either shifting or disappearing, and may be quantitatively connected with the Hg^{2+} concentration.

Selectivity of AgNPs

AgNPs' distinct molecular interaction accounts for their selectivity in the detection of Hg^{2+}. Such interactions might be assessed by colorimetric and spectrophotometric studies, which are accomplished by altering the color of AgNPs and its SPR band, respectively. In an earlier paragraph, it was stated that synthetic AgNPs had a brown water dispersion with an SPR band at 441 nm (Fig. 1). In order to conduct the detection and selectivity test, 90 μM of each of the following cations: Ba^{2+}, Ni^{2+}, Fe^{2+}, Co^{2+}, Mg^{2+}, Ca^{2+}, Pb^{2+}, and Hg^{2+} was mixed with an equal amount of AgNPs separately. For the majority of the cations, the SPR band's intensity and position remained static, as did AgNPs' color. However, for Hg^{2+}, the SPR band disappeared and AgNPs' color changed from brown to nearly colorless (Fig. 9). This result suggests that the AgNPs colorimetric nanoprobe provided Hg^{2+} detection selectivity.

In order to accurately assess this selectivity, additional comparable experiments were carried out. To make a solution containing two cations, an equal volume of 90 μM of each Hg^{2+} ion and other cations was combined separately. This combination was then mixed with an equal volume of the AgNPs dispersion separately, as previously described. The SPR band vanished in each instance (Fig. 10a), demonstrating that AgNPs could selectively detect Hg^{2+} in the presence of a single cation. In a similar manner, a solution including many cations is prepared by mixing an equal amount of 90 μM of each Hg^{2+} ion and other cation with AgNPs. The combination of additional cations did not alter the color of AgNPs or the SPR band in the absence of Hg^{2+} ions (Fig. 10b). Conversely, Hg^{2+} effectively altered the color and the SPR band of AgNPs vanished in both the presence and absence of the remaining seven cations (Fig. 10b). The aforementioned result makes it precise and clear that the green-produced AgNPs assisted by *Piper chaba* leaf extract can detect Hg^{2+} ions with great selectivity even in the presence of equimolar concentrations of other interfering cations from other metals. Numerous reports also showed comparable outcomes. The outcomes found here are comparable to those of several other published investigations.[19,44,50,68,69] The potential of *Piper chaba* leaf extract assisted

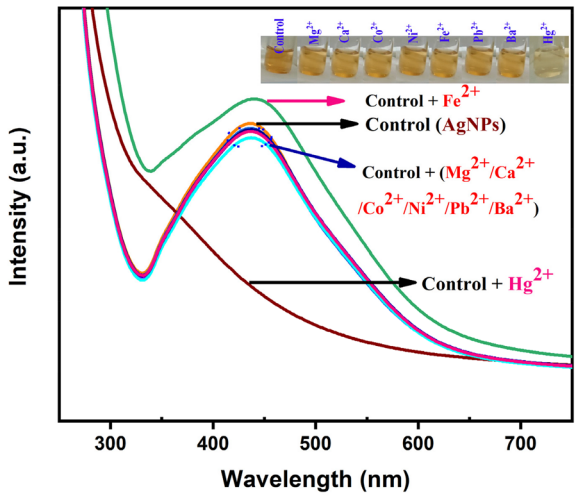

Fig. 9 Absorption spectra and visual change of AgNPs when individually exposed to various metal ions.

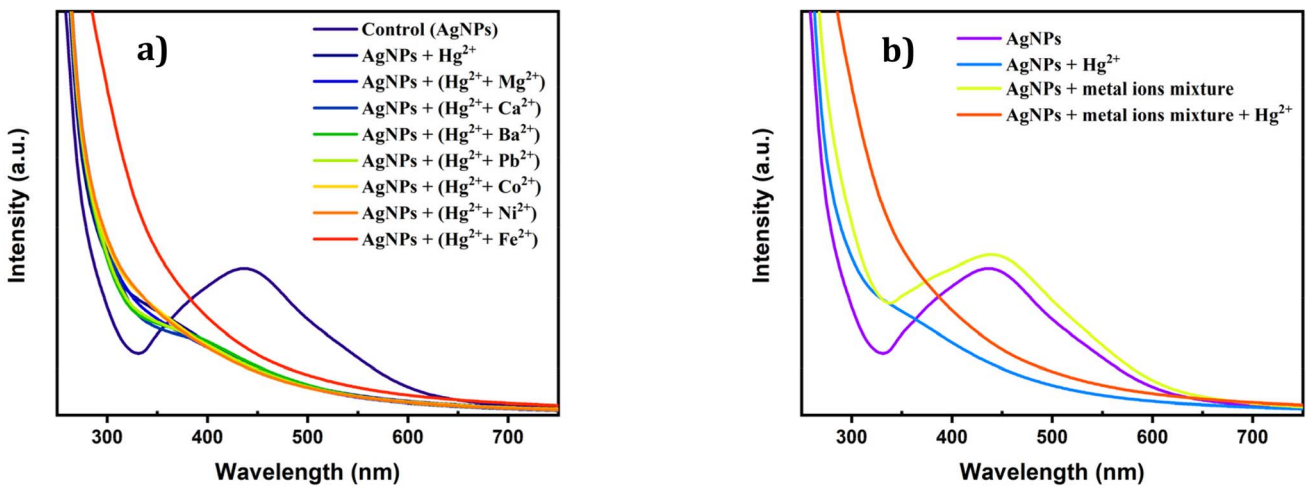

Fig. 10 Absorption spectra of AgNPs when exposed to various metal ions (a) Hg^{2+} with an individual metal ion and (b) Hg^{2+} with the mixture of metal ions.

synthesized AgNPs in wastewater treatment is enhanced by their selectivity in detecting Hg^{2+}.

Sensitivity

One important aspect of sensing analysis is the sensitivity of a detection probe. Therefore, the effect of the Hg^{2+} ion concentrations on the SPR band of AgNPs was extensively evaluated in order to estimate the sensitivity of the synthesized AgNPs for the colorimetric and spectroscopic detection of Hg^{2+} ion. The SPR absorption band of AgNPs with varying Hg^{2+} concentrations are displayed in Fig. 11; the SPR absorption band of AgNPs drastically dropped when the Hg^{2+} concentration climbed from 10 to 90 pm. The corresponding images of the detection-analyzing samples (Fig. 11) indicates that when the concentration of Hg^{2+} rose, the color of the AgNPs dispersion changed from brown to colorless. This observation, which was in line with the SPR absorption spectra, verified the relationship between the colorimetric activity of AgNPs and the concentration of Hg^{2+}. AgNPs may be employed as a colorimetric nanoprobe for quantitative Hg^{2+} detection because of the direct relationship between the quantity of Hg^{2+} and the change in the SPR band absorbance.

The equation $y = 0.0025x - 0.0072$ ($R^2 = 0.9949$) was used to compute the linear connection between the concentrations of Hg^{2+} ions and the change in the SPR band absorbance, which is shown in Fig. 12a (Hg^{2+} concentration varied from 10 to 80 μM). The limit of detection (LOD) of the AgNPs colorimetric probe was determined to be 14 μM using eqn (1) and the limit of quantification (LOQ) was determined to be 41 μM using eqn (2). Comparable sensing performance was also noted for distinct AgNPs that were synthesized using different plant sources (Table 2). Furthermore, a noticeable difference was not visible until 60 min after a quick difference was noticed in the AgNPs' SPR absorption band after 1 min (Fig. 12b). This suggested a possible use of the plant-source aided synthetic AgNPs for the unmodified fast visual colorimetric detection of Hg^{2+} ions with a notably low detection limit.

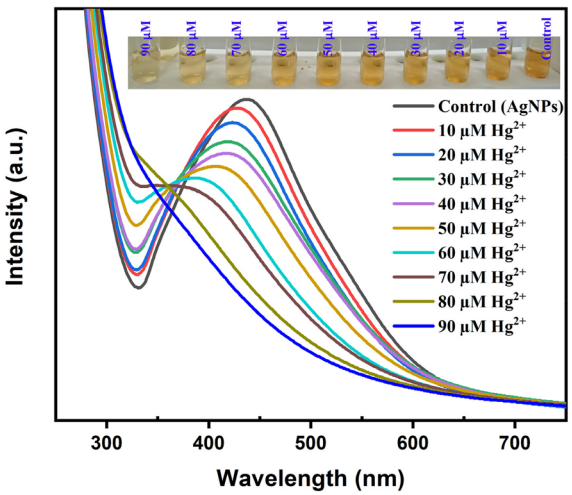

Fig. 11 Visual change and UV-vis absorption spectra of the mixtures of AgNPs and Hg^{2+} with varied Hg^{2+} concentrations (10–90 μM).

Mechanism of detection

The sensitivity of the Hg^{2+} ions detection in the presence of green synthesized AgNPs is an effective and widespread method with the advantage of a clear colorimetric mechanism through a simple redox reaction of the AgNPs and Hg^{2+} ions. Hg^{2+} ions play an important role in this redox process.[22,77,79] Owing to its high electrochemical redox potential (0.92 V), Hg^{2+} ions efficiently promote the oxidation of AgNPs (Ag^0) to Ag^+ ions (0.8 V), resulting in the mercury layer formation on the AgNPs surface and causing the optical property change of AgNPs. The color change from brown to colorless, which occurs when AgNPs interact with Hg^{2+} ions, is a vivid signal for the presence of Hg^{2+}. This change is the result of a diminution in the SPR absorption peak of the AgNPs around 441 nm. The intensity of the color

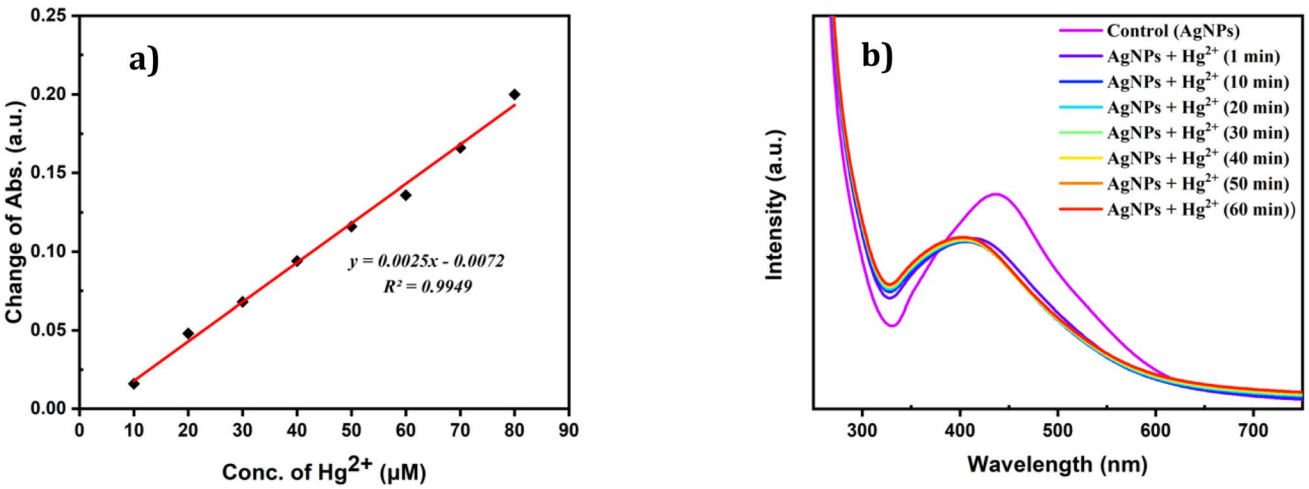

Fig. 12 (a) The regression coefficient between the change in absorbance of AgNPs and the concentration of Hg^{2+}. (b) Time-dependent UV-vis spectra of AgNPs dispersion in the presence of Hg^{2+} ions (10 μM).

Table 2 Comparison of the AgNPs synthesized in the present work with the reported green synthesized AgNPs for the colorimetric detection of Hg^{2+} ions[a]

Plant source	LOD	LOQ	Ref.
Coffea canephora fruit skin	0.039 mg L^{-1}	0.130 mg L^{-1}	70
Bell paper	0.03 μM	0.09 μM	71
Manilkara zapota L. peel	10.70 μM	32.43 μM	72
Vachellia xanthophloea	22.2 μM	73.9 μM	73
Citrus japonica leaf	0.09 μM	0.30 μM	18
Acacia raddiana leaf	1.322×10^{-5} M	4.4×10^{-5} M	74
Nannorrhops ritchiana leaf	4.8×10^{-7} M	4.8×10^{-7} M	75
Ziziphus mauritiana leaf	0.04 nM	1.5 nM	76
Acacia confusa leaf	44.3 μM	n.f.	77
Soap-root plant	2.2×10^{-6} mol L^{-1}	n.f.	17
Mimosa diplotricha leaf	2.48 μM	n.f.	78
Averrhoa bilimbi fruit	1.58 μM	5.27 μM	15
Piper chaba leaf	14 μM	41 μM	This work

[a] n.f. (not found).

change shows a linear relationship with the concentration of Hg^{2+} ions, allowing for precise quantitative determination. Moreover, the SPR behavior of AgNPs is very responsive to changes in their surface surroundings. The attachment of Hg^{2+} ions to AgNPs affects the localized surface plasmon resonance (LSPR) properties, resulting in a significant reduction in absorption intensity and a shift in the position of the absorption peak. This shift visually shows up as a clear and distinct color change, reinforcing the robustness of this detection mechanism.

Catalytic activity

A typical model reaction for assessing the catalytic efficacy of various metal nanoparticles, such as Ag, Au, Cu, Pt, and Pd, is the catalytic reduction of 4-nitrophenol (4-NP) to 4-aminophenol (4-AP), wherein, the decay of the 4-nitrophenolate anion allowed UV spectrophotometry to track the reduction process of 4-NP.[80,81] Accordingly, this study also focused on the catalytic activity of the *Piper chaba* leaf extract-assisted synthetic AgNPs for the reduction of 4-NP to 4-AP in the presence of sodium borohydride as a reductant, as well as the degradation of organic dyes, specifically methyl orange (MO) and methylene blue (MB). In short, an aqueous $NaBH_4$ solution that had just been prepared was added to an aqueous 4-NP solution to generate the 4-nitrophenolate anion. The solution's hue instantly changed from pale yellow to deep yellow, corresponding with the distinctive absorption peak shifting from 317 nm to 400 nm. The rich yellow hue eventually vanished upon the addition of the AgNPs, and the strength of the 4-nitrophenolate ion absorption peak progressively dropped. At 297 nm, a new peak started to emerge, and as time went on, the absorption peak's strength grew, showing that the decrease of 4-NP, which was eventually transformed to 4-AP, was progressing (Fig. 13a). The deep yellow hue remained, the 400 nm peak's intensity remained constant, and there was no peak seen at 297 nm in the absence of AgNPs. In contrast, the 400 nm peak vanished, the deep yellow hue became colorless, and the maximum intensity peak at 297 nm occurred after 10 min, indicating that 4-NP had totally converted to 4-AP.

As additional model reactions to verify the catalytic efficacy of AgNPs utilizing MO and MB, the catalytic degradation of dyes in the presence of $NaBH_4$ was investigated. This process was similar to that of 4-NP. The color of the dye solution remained unchanged and the characteristic peak's intensity remained

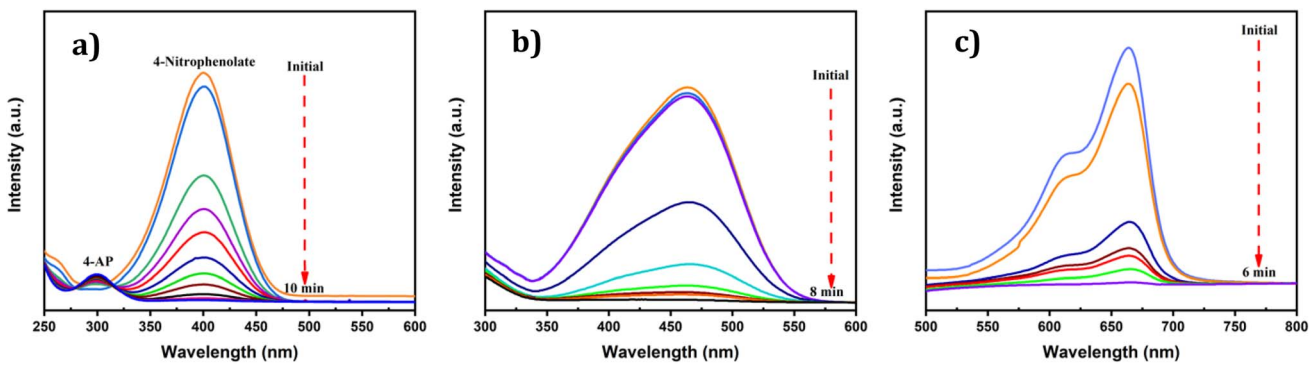

Fig. 13 Time-dependence UV-vis absorption spectra for the catalytic reduction of (a) 4-NP, (b) MO, and (c) MB by $NaBH_4$ in the presence of AgNPs synthesized using *Piper chaba* leaf extract.

constant in the absence of AgNPs after 1 h. In contrast, the characteristic peaks vanished and the dyes became colorless after a few minutes, indicating that MO and MB had totally degraded. With MO, the orange solution changed to a colorless state, while the intensity of the absorption peak at 467 nm simultaneously dropped. This outcome amply illustrates the *Piper chaba* leaf extract assisted the synthesized AgNPs' catalytic activity (Fig. 13b). The MO underwent quantitative degradation after 8 min, and its catalytic capacity is similar to the previously reported dispersion of almost identically sized biogenically produced AgNPs.[41] Conversely, the deep blue color of MB changed to colorless, while the intensity of the absorption peak at 665 nm simultaneously dropped. This outcome also amply illustrates that the *Piper chaba* leaf extract assisted with the synthesized AgNPs' catalytic activity (Fig. 13c). The MB underwent quantitative degradation after 6 min, and its catalytic capacity is also similar to the previously reported dispersion of almost identically sized biogenically produced AgNPs.[41]

In the present work, as indicated in previous works,[35,82–85] the catalytic reduction of 4-NP to 4-AP using an excess amount of $NaBH_4$ in the presence of AgNPs is considered a model reaction to evaluate the catalytic efficacy of green-synthesized AgNPs. The thermodynamically favorable but kinetically unfavorable reduction of 4-NP to 4-AP could take place in the presence of AgNPs as a catalyst. It can be assumed that the reduction occurred *via* the Langmuir–Hinshelwood mechanism. One possible explanation is that the 4-NP and borohydride ions (BH_4^-) first adsorb on the surface of the AgNPs, then the donor BH_4^- relays electrons to the acceptor 4-NP, which is converted to 4-AP and desorbs from the AgNPs' surface to make the AgNPs' surface ready for the next catalytic cycles. At the same time, it can be assumed that the catalytic degradation of MO and MB occurred *via* the same mechanism.

The reaction kinetics were monitored from time-dependent adsorption data. It should be assumed that the reaction follows pseudo-first order kinetics, because the concentration of $NaBH_4$ is higher than that of 4-NP.[82,86] Therefore, the pseudo-first order rate constants (k) of the reaction were calculated from the linear fitting of the plot of $\ln(A/A_o)$ *versus* t (min) (Fig. 14a), where A_o and A are the absorbance of the organic molecules (4-

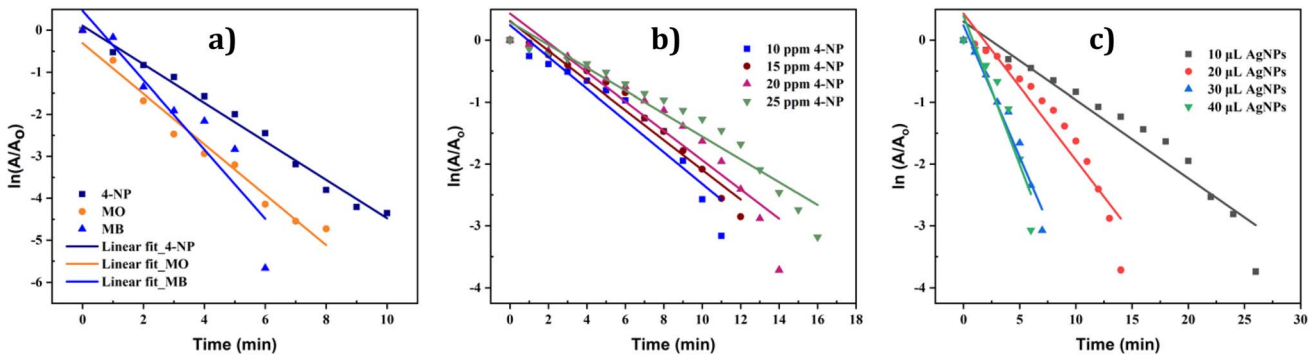

Fig. 14 Plots of $\ln(A/A_o)$ *versus* time for the catalytic reduction of (a) 4-NP, MO, and MB; (b) for the catalytic reduction of 4-NP in different concentrations of 4-NP and (c) for the catalytic reduction of 4-NP in different dosages of AgNPs.

Table 3 Comparison of the AgNPs synthesized in the present work with the reported green synthesized AgNPs for the catalytic reduction of organic dyes

Natural sources	Organic components	Rate constant	R^2	Ref.
Trigonella foenum-graecum L. leaf	Methyl orange	0.1665 min^{-1}	0.9366	49
	Methylene blue	0.1054 min^{-1}	0.9653	
	Rhodamine B	0.2004 min^{-1}	0.9838	
Sargassum serratifolium	Methyl orange	0.1580 min^{-1}	0.9317	42
	Methylene blue	0.3299 min^{-1}	0.9624	
	Rhodamine B	0.9131 min^{-1}	0.9518	
Phoenix dactylifera L.	4-Nitrophenol	0.004 s^{-1}	0.9618	87
Green coffee bean	4-Nitrophenol	0.0456 s^{-1}	0.990	45
Psidium guajava leaf	4-Nitrophenol	0.159 min^{-1}	0.975	88
Syzygium aromaticum	4-Nitrophenol	0.07494 min^{-1}	—	89
	Methylene blue	0.34493 min^{-1}	—	
	Rhodamine B	0.4431 min^{-1}	—	
Aloe vera leaf and *Cucumis sativus* leaf	Methyl orange	6.03×10^{-4} s^{-1}	—	37
	4-Nitrophenol	1.51×10^{-3} s^{-1}	—	
Piper chaba leaf	4-Nitrophenol	0.4584 min^{-1}	0.9867	This work
	Methyl orange	0.6012 min^{-1}	0.9717	
	Methylene blue	0.8263 min^{-1}	0.8455	

NP, MO, and MB) at the initial state and time t, respectively. The rate constants for 4-NP, MO, and MB were found to be 0.4584, 0.6012, and 0.8263 min^{-1}, respectively. The results are in good agreement with the reported works (Table 3).

It is well established that the reactant concentration affects the rate of a chemical reaction.[30,46,84] Here, linear fitted plots of $\ln(A/A_o)$ *vs.* time (min) have been reported for the various AgNPs and 4-NP concentrations. In order to investigate the impact of 4-NP on the reduction, initial concentrations of 10, 15, 20, and 25 ppm were used; Fig. 14b displays the outcomes. It was found that the rate constant decreased as the 4-NP concentration rose. Since reactions typically accelerate as the reactant concentration rises, this occurrence is abnormal. The reaction mechanism explains the unexpected phenomenon. A high concentration of 4-NP causes the AgNPs' surface to be almost completely covered with 4-NP, which limits the electron transition from $NaBH_4$ to 4-NP and limits the catalytic activity of $NaBH_4$.[90] In addition, the impact of the AgNPs concentrations on 4-NP reduction is depicted in Fig. 14c. As the quantity of AgNPs increased, the rate constant tended to rise.

Conclusions

In conclusion, we successfully synthesized environmentally friendly silver nanoparticles (AgNPs) using *Piper chaba* leaf extract as a natural capping and reducing agent. This green synthesis method demonstrated reduced toxicity compared to conventional approaches, making it safer for living organisms and the environment. The formation of AgNPs was visually confirmed by a color change and validated by UV-vis analysis with a surface plasmon resonance band at 441 nm. Structural analyses using SEM, TEM, and XRD revealed that the AgNPs were spherical, crystalline, and monodispersed, with an average size of 20 nm. FTIR and TG analysis confirmed the capping of the AgNPs with phytochemicals from the leaf extract, which make them stably dispersed in aqueous media. Notably, these synthesized AgNPs exhibited multifunctionality by serving as a sensitive sensing-probe for Hg^{2+} detection, characterized by color and absorption peak changes with the LOD value of 14 μM and LOQ value of 41 μM. The green synthesized AgNPs also act as an efficient nanocatalyst for the reduction of 4-NP and the degradation of organic dyes, namely MO and MB. This study highlights the potential of phytochemical-mediated AgNPs for sustainable applications in environmental monitoring and catalysis.

Consent to publish

All authors agreed with the manuscript's content and gave explicit permission to publish the work.

Conflicts of interest

The authors declare that they have no known competing financial interests or personal relationships that could have appeared to influence the work reported in this paper.

Data availability

The datasets generated and/or analyzed during the current study are available from the corresponding author on reasonable request.

Acknowledgements

The research was supported by Special Research Allocation (SRG-242287 and SRG-226666) from the Ministry of Science and Technology, Bangladesh.

References

1 P. Raveendran, J. Fu and S. L. Wallen, *J. Am. Chem. Soc.*, 2003, **125**, 13940–13941.
2 D. D. Evanoff and G. Chumanov, *ChemPhysChem*, 2005, **6**, 1221–1231.
3 L. Mulfinger, S. D. Solomon, M. Bahadory, A. V. Jeyarajasingam, S. A. Rutkowsky and C. Boritz, *J. Chem. Educ.*, 2007, **84**, 322.
4 S. P. Dubey, M. Lahtinen and M. Sillanpää, *Process Biochem.*, 2010, **45**, 1065–1071.
5 V. S. Saji, H. C. Choe and K. W. K. Yeung, *Int. J. Nano Biomater.*, 2010, **3**, 119.
6 T. Bora and J. Dutta, *J. Nanosci. Nanotechnol.*, 2014, **14**, 613–626.
7 F. J. Heiligtag and M. Niederberger, *Mater. Today*, 2013, **16**, 262–271.
8 S. A. M. Ealia and M. P. Saravanakumar, *IOP Conf. Ser.: Mater. Sci. Eng.*, 2017, **263**, 032019.
9 M. A. Albrecht, C. W. Evans and C. L. Raston, *Green Chem.*, 2006, **8**, 417.
10 J. Xie, J. Y. Lee, D. I. C. Wang and Y. P. Ting, *ACS Nano*, 2007, **1**, 429–439.
11 A. Kumar, P. K. Vemula, P. M. Ajayan and G. John, *Nat. Mater.*, 2008, **7**, 236–241.
12 P. V. AshaRani, G. L. K. Mun, M. P. Hande and S. Valiyaveettil, *ACS Nano*, 2009, **3**, 279–290.
13 A. Bastiansz, J. Ewald, V. R. Saldaña, A. Santa-Rios and N. Basu, *Environ. Health Perspect.*, 2022, **130**, 1–11.
14 S. Pramanik, M. Kumar and A. Qureshi, *Regul. Toxicol. Pharmacol.*, 2021, **121**, 104870.
15 M. T. Islam, S. K. Das, M. A. M. Nahim, M. R. Karim, R. Kundu, M. A. R. Khan, S. Rahman, M. Al-Gawati, A. N. Alodhayb and H. M. Ahsan, *RSC Adv.*, 2025, **15**, 10074–10084.
16 N. C. Pomal, K. D. Bhatt, K. M. Modi, A. L. Desai, N. P. Patel, A. Kongor and V. Kolivoška, *J. Fluoresc.*, 2021, **31**, 635–649.
17 K. Farhadi, M. Forough, R. Molaei, S. Hajizadeh and A. Rafipour, *Sens. Actuators, B*, 2012, **161**, 880–885.
18 S. Bhagat, H. Shaikh, A. Nafady, Sirajuddin, S. T. H. Sherazi, M. I. Bhanger, M. R. Shah, M. I. Abro, R. Memon and R. Bhagat, *J. Cluster Sci.*, 2022, **33**, 1865–1875.
19 P. Saha, M. M. Billah, A. B. M. N. Islam, M. A. Habib and M. Mahiuddin, *Glob. Chall.*, 2023, 2300072.

20 K. T. Tam, N. T. Thuy, N. T. K. Ngan, N. M. Khai and D. V. Thanh, *R. Soc. Open Sci.*, 2023, **10**(2), 220819.
21 T. J. Jayeoye, F. N. Eze, O. O. Olatunde, S. Singh, J. Zuo and O. J. Olatunji, *Int. J. Nanomed.*, 2021, **16**, 7557–7574.
22 N. M. Abbasi, M. U. Hameed, N. Nasim, F. Ahmed, F. Altaf, S. Shahida, S. Fayyaz, S. M. Sabir and P. Bocchetta, *Coatings*, 2022, **12**, 763.
23 Y. Zou, J. Pang, F. Zhang and F. Chai, *ChemistrySelect*, 2021, **6**, 6077–6082.
24 M. Chahar, S. Khaturia, H. L. Singh, V. S. Solanki, N. Agarwal, D. K. Sahoo, V. K. Yadav and A. Patel, *Front. Environ. Sci.*, 2023, **11**, 1–24.
25 A. Roy, A. Sharma, S. Yadav, L. T. Jule and R. Krishnaraj, *Bioinorg. Chem. Appl.*, 2021, **2021**, 1–16.
26 R. A. Kristanti, T. Hadibarata, A.-G. Niculescu, D. E. Mihaiescu and A. M. Grumezescu, *Nanomaterials*, 2025, **15**, 1133.
27 R. Saxena, M. Saxena and A. Lochab, *ChemistrySelect*, 2020, **5**, 335–353.
28 F. J. Alguacil, M. Alonso and J. I. Robla, *Int. J. Mol. Sci.*, 2024, **25**, 9671.
29 A. Tiwari, V. Sandhwar, S. Saxena, D. Saxena and G. Damle, *Discov. Sustain.*, 2025, **6**, 636.
30 L. David and B. Moldovan, *Nanomaterials*, 2020, **10**, 202.
31 I. S. Yunus, Harwin, A. Kurniawan, D. Adityawarman and A. Indarto, *Environ. Technol. Rev.*, 2012, **1**, 136–148.
32 U. Shanker, M. Rani and V. Jassal, *Environ. Chem. Lett.*, 2017, **15**, 623–642.
33 M. Mahiuddin, P. Saha and B. Ochiai, *Nanomaterials*, 2020, **10**, 1777.
34 M. MeenaKumari and D. Philip, *Spectrochim. Acta, Part A*, 2015, **135**, 632–638.
35 M. Ismail, M. I. Khan, S. B. Khan, K. Akhtar, M. A. Khan and A. M. Asiri, *J. Mol. Liq.*, 2018, **268**, 87–101.
36 M. Nasrollahzadeh, S. M.-G. Yek, N. Motahharifar and M. G. Gorab, *Chem. Rec.*, 2019, **19**, 2436–2479.
37 M. Riaz, U. Sharafat, N. Zahid, M. Ismail, J. Park, B. Ahmad, N. Rashid, M. Fahim, M. Imran and A. Tabassum, *ACS Omega*, 2022, **7**, 14723–14734.
38 H. Duan, D. Wang and Y. Li, *Chem. Soc. Rev.*, 2015, **44**, 5778–5792.
39 I. Ijaz, E. Gilani, A. Nazir and A. Bukhari, *Green Chem. Lett. Rev.*, 2020, **13**, 223–245.
40 C. Vanlalveni, S. Lallianrawna, A. Biswas, M. Selvaraj, B. Changmai and S. L. Rokhum, *RSC Adv.*, 2021, **11**, 2804–2837.
41 P. Saha, M. Mahiuddin, A. B. M. N. Islam and B. Ochiai, *ACS Omega*, 2021, **6**, 18260–18268.
42 B. Kim, W. C. Song, S. Y. Park and G. Park, *Catalysts*, 2021, **11**, 347.
43 F. Ahmed, H. Kabir and H. Xiong, *Front. Chem.*, 2020, **8**, 1–15.
44 S. S. Ravi, L. R. Christena, N. SaiSubramanian and S. P. Anthony, *Analyst*, 2013, **138**, 4370.
45 M. Wang, W. Zhang, X. Zheng and P. Zhu, *RSC Adv.*, 2017, **7**, 12144–12149.
46 S. Joseph and B. Mathew, *J. Mol. Liq.*, 2015, **204**, 184–191.
47 J. Saha, A. Begum, A. Mukherjee and S. Kumar, *Sustain. Environ. Res.*, 2017, **27**, 245–250.
48 H. Veisi, S. Azizi and P. Mohammadi, *J. Clean. Prod.*, 2018, **170**, 1536–1543.
49 M. Moond, S. Singh, S. Sangwan, P. Devi, A. Beniwal, J. Rani, A. Kumari and S. Rani, *Molecules*, 2023, **28**, 951.
50 A. Adhikari, L. Lamichhane, A. Adhikari, G. Gyawali, D. Acharya, E. R. Baral and K. Chhetri, *Inorganics*, 2022, **10**, 113.
51 P. Saha, M. Mahiuddin, A. B. M. N. Islam and B. Ochiai, *ACS Omega*, 2021, **6**, 18260–18268.
52 M. M. Rahman, T. T. Dipti, M. N. Islam, A. T. M. Abdullah, S. Jahan, M. M. Alam and M. R. Karim, *Saudi J. Biol. Sci.*, 2023, **30**, 103663.
53 M. E. Haque, M. Rani and A. C. Roy, Rev. Phytochem. Pharmacol. Investig. Piper chaba Hunt., *Int. J. Sci. Eng. Res.*, 2018, **9**, 937–941.
54 V. R. S. Rao, G. Suresh, K. S. Babu, S. S. Raju, M. V. P. S. Vishnu Vardhan, S. Ramakrishna and J. M. Rao, *Tetrahedron*, 2011, **67**, 1885–1892.
55 M. Ansari, S. Ahmed, A. Abbasi, M. T. Khan, M. Subhan, N. A. Bukhari, A. A. Hatamleh and N. R. Abdelsalam, *Sci. Rep.*, 2023, **13**, 18048.
56 W. W. Melkamu and L. T. Bitew, *Heliyon*, 2021, **7**, e08459.
57 J. Huang, Q. Li, D. Sun, Y. Lu, Y. Su, X. Yang, H. Wang, Y. Wang, W. Shao, N. He, J. Hong and C. Chen, *Nanotechnology*, 2007, **18**, 105104.
58 J. Huang, G. Zhan, B. Zheng, D. Sun, F. Lu, Y. Lin, H. Chen, Z. Zheng, Y. Zheng and Q. Li, *Ind. Eng. Chem. Res.*, 2011, **50**, 9095–9106.
59 N. Liaqat, N. Jahan, Khalil-ur-Rahman, T. Anwar and H. Qureshi, *Front. Chem.*, 2022, **10**, 1–13.
60 K. Sharma, S. Guleria and V. K. Razdan, *J. Plant Biochem. Biotechnol.*, 2020, **29**, 213–224.
61 N. Sangeetha, S. Manikandan, M. Singh and A. K. Kumaraguru, *Curr. Nanosci.*, 2012, **8**, 697–702.
62 E. C. Njagi, H. Huang, L. Stafford, H. Genuino, H. M. Galindo, J. B. Collins, G. E. Hoag and S. L. Suib, *Langmuir*, 2011, **27**, 264–271.
63 M. Vanaja and G. Annadurai, *Appl. Nanosci.*, 2013, **3**, 217–223.
64 T. Rukachaisirikul, S. Prabpai, P. Champung and A. Suksamrarn, *Planta Med.*, 2002, **68**, 853–855.
65 S. M. Bis, N. Chakrabort, P. Chakrabort and S. Sarkar, *Res. J. Med. Plant*, 2012, **6**, 574–586.
66 A. C. Roy, M. E. Haque, S. Rahman, M. A. Al-Mansur and C. M. E. Haque, *J. Pharmacogn. Phytochem.*, 2018, **7**, 2653–2662.
67 R. F. Hamdi, *Bionanoscience*, 2025, **15**(3), 341.
68 T. J. Jayeoye, F. N. Eze, O. J. Olatunji and A. A. Tyopine, *Sci. Rep.*, 2022, **12**, 9176.
69 B. Prosposito, L. Burratti, A. Bellingeri, G. Protano, C. Faleri, I. Corsi, C. Battocchio, G. Iucci, L. Tortora, V. Secchi, S. Franchi and I. Venditti, *Nanomaterials*, 2019, **9**(10), 1353.
70 H. Sulistyarti, M. M. Utama, A. M. Fadhila, A. Cahyaningrum, R. J. Murti and A. Febriyanti, *Anal. Sci.*, 2023, **39**, 335–346.

71 A. Khatoon, J. A. Syed, J. A. Buledi, S. Shakeel, A. Mallah, A. R. Solangi, Sirajuddin, S. T. H. Sherazi and M. R. Shah, *J. Iran. Chem. Soc.*, 2022, **19**, 3659–3672.
72 A. Beniwal, S. Singh, J. Rani, M. Moond, S. Kakkar, S. Sangwan and S. Kumari, *Discover Nano*, 2024, **19**(1), 191.
73 A. J. Mwakalesi, *Plasmonics*, 2023, **18**, 2077–2090.
74 N. H. Ibrahim, G. M. Taha, N. S. A. Hagaggi and M. A. Moghazy, *BMC Chem.*, 2024, **18**, 7.
75 S. Khan, S. Shujah, U. Nishan, S. Afridi, M. Asad, A. ul, H. A. Shah, N. Khan, S. Ramzan and M. Khan, *Arabian J. Sci. Eng.*, 2023, **48**, 7673–7684.
76 R. Memon, A. A. Memon, Sirajuddin, A. Balouch, K. Memon, S. T. H. Sherazi, A. A. Chandio and R. Kumar, *Int. J. Environ. Anal. Chem.*, 2022, **102**, 7046–7061.
77 A. Kalam, A. G. Al-Sehemi, M. Ashrafuzzaman, A. M. Sharif, P. Yadav and G. Du, *Bull. Chem. Soc. Ethiop.*, 2023, **37**, 1287–1298.
78 M. S. Punnoose, D. Bijimol, T. Abraham, N. J. Plathanam and B. Mathew, *Bionanoscience*, 2021, **11**, 739–754.
79 V. Kumar, D. K. Singh, S. Mohan, D. Bano, R. K. Gundampati and S. H. Hasan, *J. Photochem. Photobiol., B*, 2017, **168**, 67–77.
80 S. Saha, A. Pal, S. Kundu, S. Basu and T. Pal, *Langmuir*, 2010, **26**, 2885–2893.
81 S. Wunder, F. Polzer, Y. Lu, Y. Mei and M. Ballauff, *J. Phys. Chem. C*, 2010, **114**, 8814–8820.
82 Y. A. Aggour, E. R. Kenawy, M. Magdy and E. Elbayoumy, *RSC Adv.*, 2024, **14**, 30127–30139.
83 A. O. C. Juarez, E. I. O. Lopez, M. K. Kesarla and N. K. R. Bogireddy, *ACS Omega*, 2024, **9**, 33335–33350.
84 R. Rajamanikandan, K. Shanmugaraj and M. Ilanchelian, *J. Cluster Sci.*, 2017, **28**, 1009–1023.
85 Y. R. Mejía and N. K. R. Bogireddy, *RSC Adv.*, 2022, **12**, 18661–18675.
86 T. M.-T. Nguyen, T. T.-T. Huynh, C.-H. Dang, D.-T. Mai, T. T.-N. Nguyen, D.-T. Nguyen, V.-S. Dang, T.-D. Nguyen and T.-D. Nguyen, *Res. Chem. Intermed.*, 2020, **46**, 1975–1990.
87 H. Al-Shwyeh, *J. Pharm. BioAllied Sci.*, 2019, **11**, 1.
88 J. Kaur, J. Singh and M. Rawat, *SN Appl. Sci.*, 2019, **1**, 1060.
89 B. Ajitha, Y. A. K. Reddy, Y. Lee, M. J. Kim and C. W. Ahn, *Appl. Organomet. Chem.*, 2019, **33**, e4867.
90 F. Xia, X. Xu, X. Li, L. Zhang, L. Zhang, H. Qiu, W. Wang, Y. Liu and J. Gao, *Ind. Eng. Chem. Res.*, 2014, **53**, 10576–10582.